Measurement of the Relative Permittivity of the Lungs During Breathing

Zhassulan Mendakulov , Ivan Vassilyev , Gulstan Yessetova , Kaiyrtay Issabayev *

Posted Date: 21 April 2026

doi: 10.20944/preprints202604.1500.v1

Keywords: antenna; auscultation; visualization; Helmholtz equation; relative permittivity; lungs; pulmonogram; radio-waves; USRP; GNU Radio

 doi:10.20944/preprints202604.1500.v1

Article

Measurement of the Relative Permittivity of the Lungs During Breathing

Zhassulan Mendakulov [1], Ivan Vassilyev [1], Gulstan Yessetova [2] and Kaiyrtay Issabayev [3,*]

[1] Special Design and Technology Bureau "Granit", 292 Hussainov Street, 050060, Almaty, Kazakhstan

[2] Kazakh National Medical University named after S.D. Asfendiyarov, Pulmonology department, 112 Ayteke bi Street, 050000, Almaty, Kazakhstan

[3] Military Engineering Institute of Radio Electronics and Communication, 53 Zhandosov Street, 050035, Almaty, Kazakhstan

* Correspondence: rtv_nk@mail.ru

Abstract

The radio-wave method for monitoring bronchopulmonary function is attractive due to its simplicity of implementation and safety for patients. The achieved results in *imaging* the lung air-filling process were encouraging; however, they also revealed several limitations that hinder the development of the method as a diagnostic tool. This paper describes an improved setup for radio-wave monitoring of the breathing process, enabling the measurement of not only amplitude but also phase pulmonograms. The setup is based on the USRP device PlutoSDR and the GNU Radio framework. Using the Helmholtz equations, it was possible to separate the contributions to amplitude and phase variations in the pulmonograms into those associated with changes in lung size during breathing and those related to changes in relative permittivity due to lung aeration. The values of relative permittivity at selected measurement points may serve as a basis for developing diagnostic indicators of various bronchopulmonary diseases. The problem of selecting these measurement points is discussed, drawing an analogy with auscultation points, but focusing on locations that provide information about the lung air filling process. The estimated measurement accuracy indicates that a single breathing cycle is sufficient to determine the relative permittivity at each measurement point.

Keywords: antenna; auscultation; visualization; Helmholtz equation; relative permittivity; lungs; pulmonogram; radio-waves; USRP; GNU Radio

1. Introduction

Respiratory diseases are among the most common diseases worldwide [1]. According to the World Health Organization (WHO), nearly 15 million people died during the COVID-19 pandemic [2]. Estimates of the number of deaths caused by the "Spanish flu" during World War I vary widely, but are commonly placed at around 50 million people [3].

A major factor contributing to the widespread prevalence of bronchopulmonary diseases is their late detection [4,5], as patients may be unaware of their illness at the early stages of many diseases [6]. Early detection of bronchopulmonary diseases facilitates treatment and improves recovery outcomes [7,8]. One of the effective approaches of combating with respiratory diseases is regular preventive screening (especially in high-risk groups), including fluorography examinations.

X-ray, fluorography, and, in recent decades, MRI are effective methods for detecting diseases [9]; however, they require relatively complex, expensive, and not entirely safe equipment. For this reason, such equipment is rarely used during mass preventive examinations.

Ongoing research is focused on the development of devices and methods capable of non-invasively and safely detecting abnormalities in the human respiratory system at an early stage, which could be used during mass preventive examinations. Promising approaches for rapid diagnostics include electrical impedance methods [10] and radio-wave diagnostic methods [11,12].

 doi:10.20944/preprints202604.1500.v1

In [13], the feasibility of *imaging* the lung air-filling process using a simple and low-cost radio-wave setup was demonstrated. The system enabled more than 50 measurements per breathing cycle across eight regions of the chest, making it possible to detect non-uniform air filling in different lung lobes, as well as to observe that some lung regions may not always be fully aerated during breathing even in healthy subjects. At the same time, this setup, which was developed as a research prototype, exhibited several limitations that hindered its effective application.

First, the simplified electrical model of the chest, although useful for understanding the principles of the radio-wave method, was not suitable for deriving objective physiological parameters from the measurement results. Second, the setup was narrowband and did not allow evaluation of the frequency dependence of the measured parameters, which could provide additional diagnostic information. Third, during the experiments, the subject was not physically fixed, as is typically done in procedures such as fluorography. This led to distortions in the pulmonograms caused by movements of the human body relative to the antennas. As a result, it was necessary to apply synchronization of inhalation and exhalation using program-generated signals and to average the pulmonograms over multiple breathing cycles.

This paper presents the results obtained in the course of improving the radio-wave method aimed at enhancing the quality and informativeness of the pulmonograms.

2. Materials and Methods

Through-transmission radio-wave scanning of the torso makes it possible to investigate the air filling of different regions of the lungs *by* analyzing *changes in the parameters* of radio waves within the lungs *during breathing*.

Assuming the human torso to be a macroscopically charge-free lossy dielectric medium, the behavior of radio waves within it can be described by the vector Helmholtz equation [14]:

$$\nabla^2 \mathbf{E}_s - \gamma^2 \mathbf{E}_s = 0 \tag{1}$$

where the electric field component of the electromagnetic wave generated by the source is represented in phasor form as $\mathbf{E}_s(x, y, z)$, depending only on the spatial coordinates. Equation (1) in the Cartesian coordinate system is equivalent to three scalar equations for the components of $\mathbf{E}$ directed along the unit vectors $\mathbf{a}_x$, $\mathbf{a}_y$ and $\mathbf{a}_z$. Let us introduce a local Cartesian coordinate system by placing the source of radiation (transmitting antenna) at the point $x = y = z = 0$ (Figure 1).

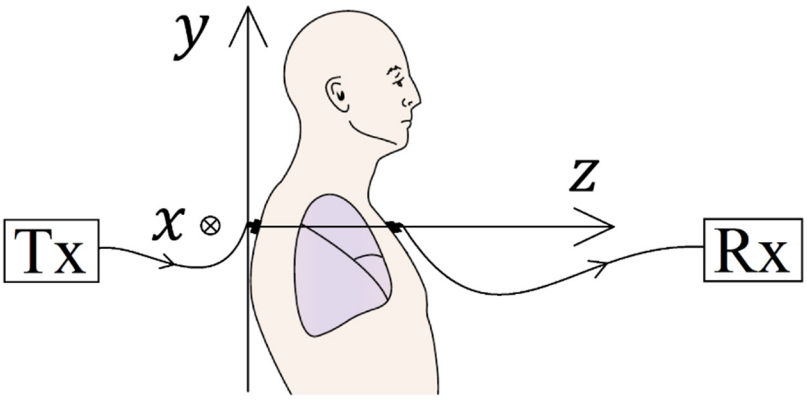

Figure 1. Positioning of the object under test relative to the coordinate system between the transmitting (Tx) and receiving (Rx) antennas.

Using antennas with horizontal polarization ($\mathbf{E}_s$ has only an x component) and placing the receiving antenna along the z axis ($x = y = 0$), the electric field can be expressed as $\mathbf{E}_s = E_{xs}(z)\mathbf{a}_x$ and in this case, the solution of Equation (1) can be written in the form of Expression (2):

$$E_{xs}(z) = C_1 e^{-\gamma z} + C_2 e^{\gamma z} \tag{2}$$

 doi:10.20944/preprints202604.1500.v1

where C_1 and C_2 are constants, determined by the boundary conditions, and the coefficient γ, defined by the parameters of the radio-wave propagation medium, is a complex quantity [15]:

$$\gamma = \alpha + j\beta$$

$$\alpha = \omega \sqrt{\frac{\mu\varepsilon}{2}\left[\sqrt{1+\left[\frac{\sigma}{\omega\varepsilon}\right]^2}-1\right]} \tag{3}$$

$$\beta = \omega \sqrt{\frac{\mu\varepsilon}{2}\left[\sqrt{1+\left[\frac{\sigma}{\omega\varepsilon}\right]^2}+1\right]} \tag{4}$$

As follows from Expressions (3) and (4), the coefficients α and β, describing the variation of the amplitude and phase of the electromagnetic wave in space, depend on the parameters of the propagation medium (absolute permittivity ε, permeability μ, electrical conductivity σ) and on the angular frequency ω.

The first term in Expression (2) describes the behavior of an electromagnetic wave propagating along the z axis in the $+z$ direction. The second term corresponds to an electromagnetic wave traveling in the opposite direction $-z$. Since, in the considered case, the signal source is located at $z = 0$, only the first term of the expression is of interest. To eliminate the influence of the second term on the measurement results, it is necessary to exclude the presence of other signal sources radiating electromagnetic waves in the $-z$ direction, as well as to suppress reflections of the wave propagating in the $+z$ direction at the location of the receiving antenna. This can be achieved by conducting measurements in environments with low external electromagnetic field and by using well-matched antennas (SWR < 2). Under these conditions, the constant C_2 can be set to zero. The solution of Equation (1) then takes the form:

$$E_{xs}(z) = C_1 e^{-\gamma z} = A e^{-\alpha z} e^{-j\beta z} e^{j\varphi_0} \tag{5}$$

where $C_1 = A e^{j\varphi_0}$ represents the signal amplitude A at the point $z = 0$ with initial phase φ_0.

Expression (5) describes the dependence of the radio wave on the parameters of the medium, i.e., the parameters of the object under investigation.

The real part of Expression (5), for a wave propagating along the $+z$ axis, can be written as:

$$\Re\{E_{xs}(z)\} = A e^{-\alpha z} \cos(-\beta z + \varphi_0) \tag{6}$$

where $A e^{-\alpha z}$ describes the attenuation of the signal amplitude A with attenuation coefficient α [$^{\mathrm{Np}}/_{\mathrm{m}}$]; $\cos(-\beta z + \varphi_0)$ represents the real part of the field, whose phase variation along the z axis is given by $-\beta z + \varphi_0$, where β is the wavenumber [$^{\mathrm{rad}}/_{\mathrm{m}}$], and φ_0 is the initial phase shift [rad].

During breathing, the geometric dimensions and electrical properties of the lungs vary at each moment in time t_{Breath}, while the magnetic permeability remains unchanged, since biological tissues can be considered non-magnetic:

$$\Delta d(t_{Breath}) = d_{in} - d_{ex}$$

$$\Delta\varepsilon_r(t_{Breath}) = \varepsilon_{r,in} - \varepsilon_{r,ex}$$

$$\Delta\sigma(t_{Breath}) = \sigma_{in} - \sigma_{ex}$$

$$\mu_r \approx 1$$

$$\mu \cong \mu_0$$

where d_{in} [m], $\varepsilon_{r,in}$ and σ_{in} [$^{\mathrm{S}}/_{\mathrm{m}}$] denote the thickness, relative permittivity and electrical conductivity of the lungs during inhalation (in), respectively; d_{ex} [m], $\varepsilon_{r,ex}$ and σ_{ex} [$^{\mathrm{S}}/_{\mathrm{m}}$] denote the thickness, relative permittivity and electrical conductivity of the lungs during exhalation (ex), respectively; and t_{Breath} [s] denotes the breathing time instant.

 doi:10.20944/preprints202604.1500.v1

The relative permittivity of the lungs $\varepsilon_{r,in}$ at the moment of inhalation (in) can serve as a *criterion for assessing* lung air filling, *provided* that the influence of chest motion on the measurement results is *eliminated*.

The calculation of the relative permittivity of the lungs $\varepsilon_{r,in}$ at the moment of inhalation (in) can be performed in several steps:

1) At the first step, the ratio of signal magnitudes Mag_{ratio} and the difference of phases Ph_{diff} [°] obtained during inhalation (in) and exhalation (ex) are determined:

$$\mathrm{Mag}_{ratio} = \frac{\mathbf{E}_0 e^{-\alpha_{in} d_{in}}}{\mathbf{E}_0 e^{-\alpha_{ex} d_{ex}}}$$

$$\mathrm{Mag}_{ratio} = e^{\alpha_{ex} d_{ex} - \alpha_{in} d_{in}}$$

$$\ln \mathrm{Mag}_{ratio} = \alpha_{ex} d_{ex} - \alpha_{in} d_{in} \tag{7}$$

$$\mathrm{Ph}_{diff} = \left((-\beta_{in} d_{in}) - (-\beta_{ex} d_{ex})\right) \frac{180}{\pi}$$

$$\mathrm{Ph}_{diff} = (\beta_{ex} d_{ex} - \beta_{in} d_{in}) \frac{180}{\pi} \tag{8}$$

2) At the second step, the values of the magnitude ratio Mag_{ratio} and the phase difference Ph_{diff} obtained during inhalation (in) and exhalation (ex) are decomposed into contributions associated with the medium and with the propagation distance.

For this purpose, average values and variations Δ: of the distance d and the coefficients α and β, which are related to the medium parameters, are introduced:

$$\bar{d} = \frac{d_{in} + d_{ex}}{2}$$

$$\Delta d = d_{in} - d_{ex}$$

$$\bar{\alpha} = \frac{\alpha_{in} + \alpha_{ex}}{2}$$

$$\Delta \alpha = \alpha_{in} - \alpha_{ex}$$

$$\bar{\beta} = \frac{\beta_{in} + \beta_{ex}}{2}$$

$$\Delta \beta = \beta_{in} - \beta_{ex}$$

Under the assumptions $|\Delta d| \ll \bar{d}$, $|\Delta \alpha| \ll \bar{\alpha}$ and $|\Delta \beta| \ll \bar{\beta}$, the values corresponding to inhalation (in) and exhalation (ex) can be approximated by their mean values. In this case, a linear decomposition of "distance vs medium" around the mean values can be expressed as:

$$\ln \mathrm{Mag}_{ratio} \approx \ln(\mathrm{Mag}_{ratio})_{dist} + \ln(\mathrm{Mag}_{ratio})_{prop} = (-\bar{\alpha} \Delta d) + \left(-\bar{d} \Delta \alpha\right) \tag{9}$$

$$\mathrm{Ph}_{diff} \approx \mathrm{Ph}_{diff,\,dist} + \mathrm{Ph}_{diff,\,prop} = \left(\left(-\bar{\beta} \Delta d\right) + \left(-\bar{d} \Delta \beta\right)\right) \frac{180}{\pi} \tag{10}$$

In Equations (9) and (10), when calculating the contribution due to distance, the contribution of the medium is assumed to remain unchanged and is replaced by the mean values of the coefficients for inhalation (in) and exhalation (ex), and *vice versa*.

To apply Equations (9) and (10), it is first necessary to calculate the coefficients α_{in} and β_{in} during inhalation (in):

$$\alpha_{in} = \frac{\alpha_{ex} d_{ex} - \ln \mathrm{Mag}_{ratio}}{d_{in}} \tag{11}$$

$$\beta_{in} = \frac{\beta_{ex} d_{ex} - \frac{\pi \mathrm{Ph}_{diff}}{180}}{d_{in}} \tag{12}$$

where $d_{in} = d_{ex} + \Delta d(t_{Breath})$.

 doi:10.20944/preprints202604.1500.v1

3) At the third step, the values of the coefficients α_{in} and β_{in} must be *re*calculated using the values of $\ln(\mathrm{Mag}_{ratio})_{prop}$ and $\mathrm{Ph}_{diff,\,prop}$ in order to further eliminate the influence of chest motion:

$$\alpha_{in,\,prop} = \frac{\alpha_{ex} d_{ex} - \ln(\mathrm{Mag}_{ratio})_{prop}}{d_{in}} \tag{13}$$

$$\beta_{in,\,prop} = \frac{\beta_{ex} d_{ex} - \frac{\pi \mathrm{Ph}_{diff,\,prop}}{180}}{d_{in}} \tag{14}$$

4) At the fourth step, using Equations (3) and (4):

$$\beta_{in,\,prop}{}^2 - \alpha_{in,\,prop}{}^2 = \omega^2 \mu \varepsilon$$

the desired value of the relative permittivity of the lungs $\varepsilon_{r,\,in}$ at the moment of inhalation (in) is determined, without the influence of chest motion on the measurement results:

$$\varepsilon_{r,\,in} = \frac{\beta_{in,\,prop}{}^2 - \alpha_{in,\,prop}{}^2}{\omega^2 \mu \varepsilon_0} \tag{15}$$

While the change in chest thickness associated with variations in lung volume can be measured relatively easily, the actual thickness of the lungs along the path between the transmitting and receiving antennas is *a priori* unknown. The geometric structure of the lungs is highly complex and may vary significantly between individuals, as well as change with age. Since the *primary* objective of this work is to demonstrate the *importance* of phase measurements, these parameters were treated as constants in the calculations: $d_{ex} = 0.06$ m, $d_{in} = 0.07$ m, $\Delta d = d_{in} - d_{ex} = 0.07 - 0.06 = 0.01$ m. The issue of determining these parameters will be discussed in the "Discussion" section.

The coefficients α_{ex} and β_{ex} for exhalation are calculated using Equations (3) and (4) for the values of relative permittivity $\varepsilon_{r,\,ex} = 51$ and electrical conductivity $\sigma_{ex} = 0.90$ $^{\mathrm{S}}/_{\mathrm{m}}$ of the lungs. The values of $\varepsilon_{r,\,ex}$ and σ_{ex} parameters were taken from [16].

For a frequency $f = 10^9$ Hz, the coefficient α_{ex} was calculated using Equation (3):

$$\alpha_{ex} = 2\pi 10^9 \sqrt{\frac{4\pi 10^{-7} 8.854 \times 10^{-12} 51}{2} \left[\sqrt{1 + \left[\frac{0.90}{2\pi 10^9 8.854 \times 10^{-12} 51} \right]^2} - 1 \right]} = 23.45 \ {}^{\mathrm{Np}}/_{\mathrm{m}}$$

and the coefficient β_{ex} was calculated using Equation (4):

$$\beta_{ex} = 2\pi 10^9 \sqrt{\frac{4\pi 10^{-7} 8.854 \times 10^{-12} 51}{2} \left[\sqrt{1 + \left[\frac{0.90}{2\pi 10^9 8.854 \times 10^{-12} 51} \right]^2} + 1 \right]} = 151.50 \ {}^{\mathrm{rad}}/_{\mathrm{m}}$$

For the practical implementation of the method for obtaining quantitative information on lung air filling, the measurement setup must provide the capability to measure not only variations in the amplitude of the radio-frequency signal, but also variations in its *phase*.

In the previous setup used for measurements [17], a radiosignal generator and receiver with independent reference oscillators were employed, which did not allow phase measurements to be performed. To enable phase measurements in the present experiment, a transceiver with a common quartz oscillator was used. As the hardware platform of the device, a low-cost and compact software-defined radio module, Adalm-Pluto, based on the AD9363 RF-transceiver, was selected.

Table 1 summarizes the main technical characteristics of the coherent transceiver Adalm-Pluto.

Table 1. Technical characteristics of the coherent Tx–Rx device Adalm-Pluto.

Tuning Range	from 325 MHz to 3800 MHz with 2.4 Hz Local Oscillator (LO) step size
Frequency Accuracy	±25 ppm
Tunable channel bandwidth	from 200 kHz to 20 MHz
Tx Power Output	7 dBm

 doi:10.20944/preprints202604.1500.v1

Rx Noise Figure	<3.5 dB
Dimensions	117 mm × 79 mm × 24 mm
Weight	114 g
Temperature	10°C to 40°C

As follows from Table 1, the maximum output power of the radio signal does not exceed 7 dBm (5 mW), which complies with the strict safety guidelines of ICNIRP [18].

To reduce the influence of reflections from surrounding objects, as well as interference caused by body movements relative to the measurement antennas—which prevented reliable data acquisition within a single breathing cycle [19]—special broadband antennas designed for attaching on the patient's body were developed and fabricated. A wide variety of antenna designs for biomedical applications exists [20,21]. Based on an analysis of their advantages and disadvantages, the antenna described in [22] was selected as the basis, and a number of improvements were introduced into its design [23]. The antenna structure is shown in Figure 2.

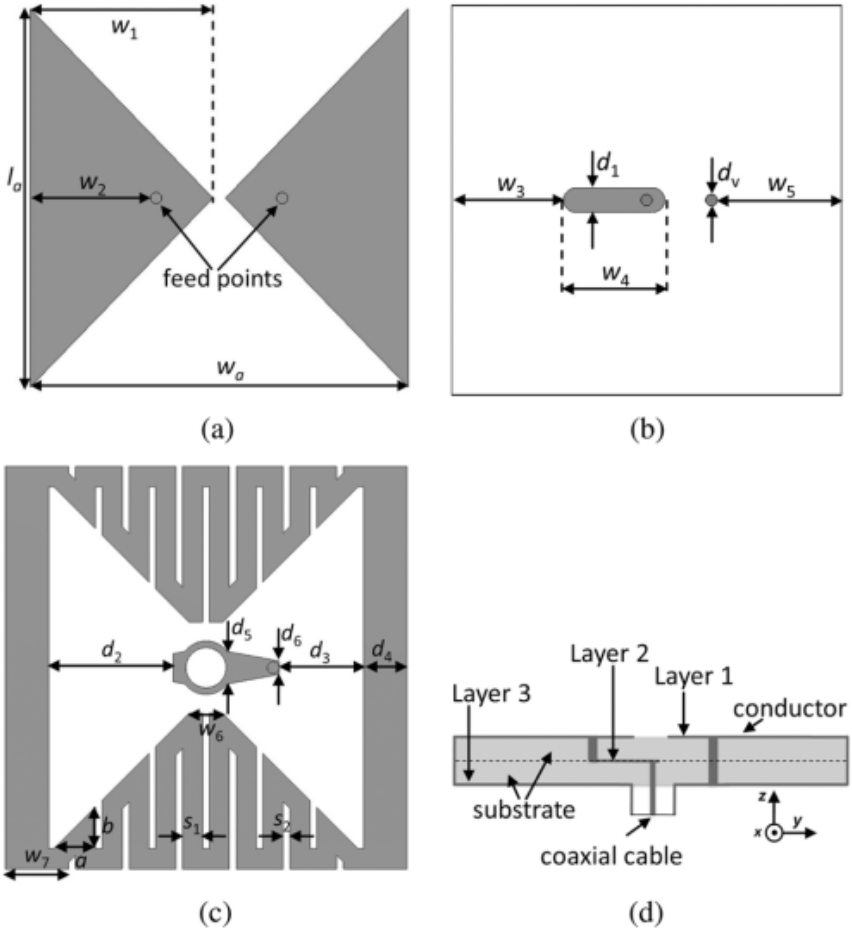

Figure 2. Design of the broadband antenna used in the experimental measurements.

The dimensions of the broadband antenna fabricated on an FR-4 substrate are presented in [24]. The English version of this paper will be published in the journal *Biomedical Engineering* (ISSN 1573-8256) in 2026. The antenna dimensions can be requested from the authors, and its appearance is shown in Figure 3.

 doi:10.20944/preprints202604.1500.v1

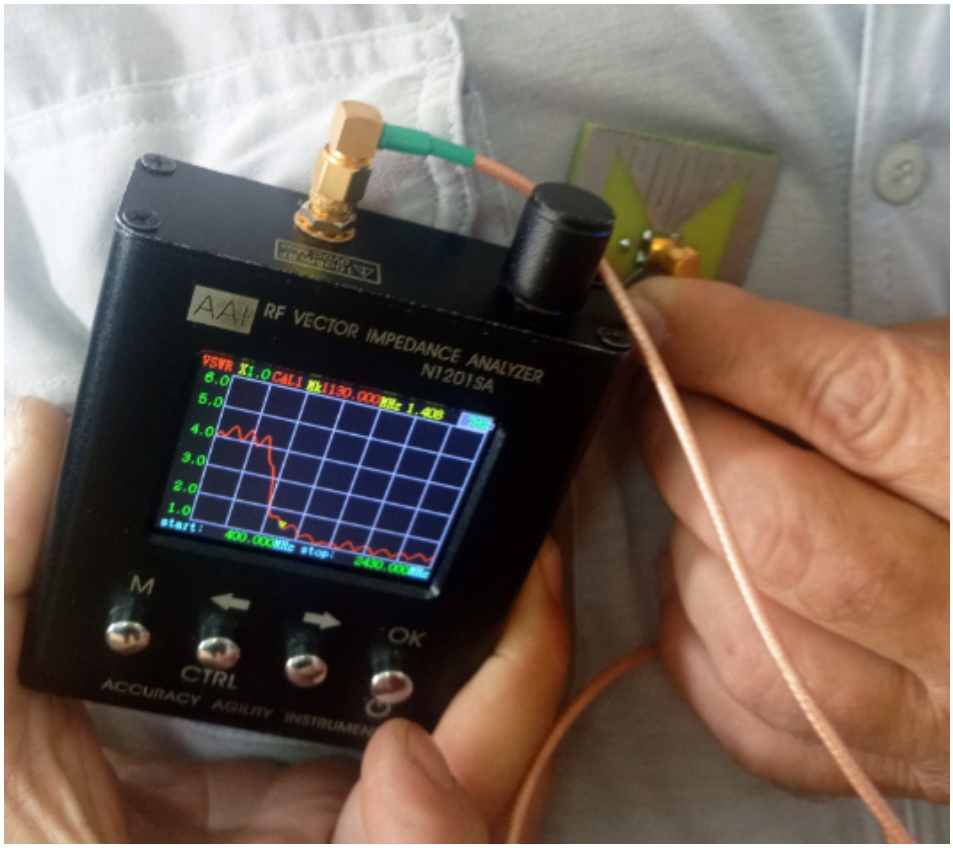

Figure 3. Broadband antenna during SWR measurements.

The results of the antenna standing wave ratio (SWR) measurements are presented in Figure 4. During the measurements, the antenna was attached in contact with the human body to simulate the conditions of pulmonogram acquisition. The antenna SWR does not exceed 2 over the frequency range from 830 MHz to 2860 MHz (Figure 4).

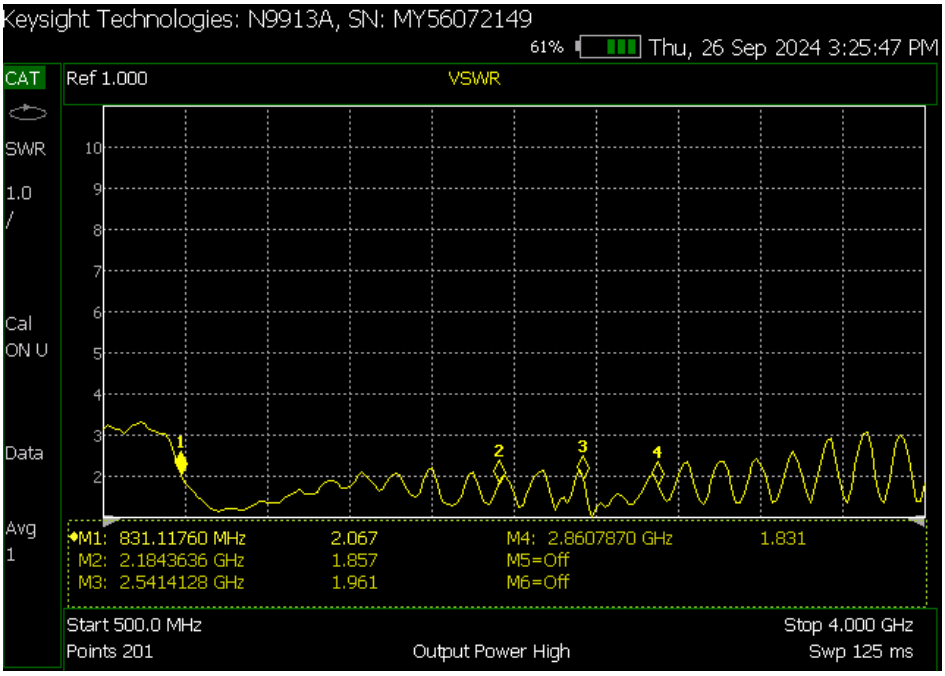

Figure 4. SWR of the broadband antenna.

 doi:10.20944/preprints202604.1500.v1

During pulmonogram measurements, the antennas were fixed on the human body at various locations over the lungs, both on the chest and on the back, using a specially designed vest with Velcro fasteners (Figure 5) to facilitate antenna positioning.

Figure 5. Attachment of antennas to the human body using an elastic vest and Velcro fasteners.

For the experiments on the study of the bronchopulmonary system, the GNU Radio framework (version 3.10.10.0) was used. This framework is widely employed by researchers for conducting various scientific experiments [25–30].

Figure 6 shows the overall flowgraph of the software developed in the GNU Radio environment.

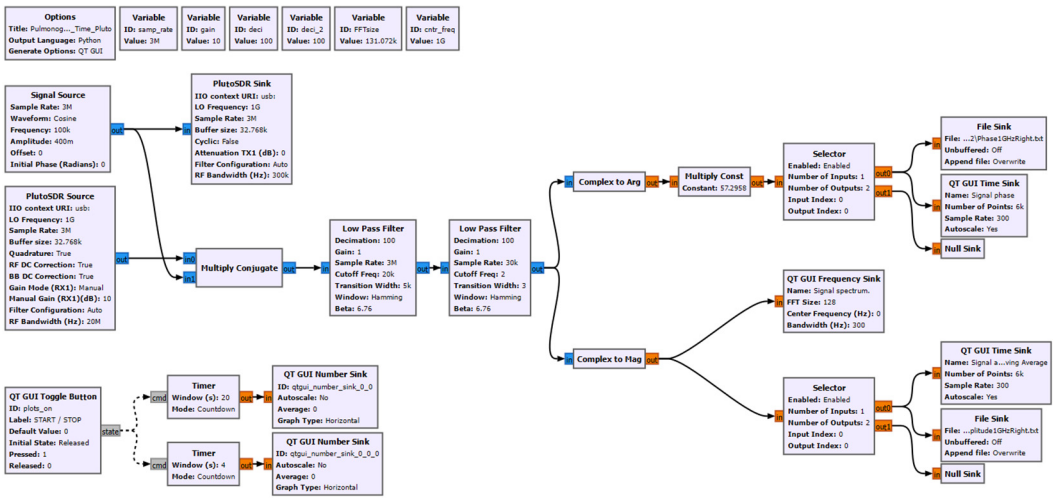

Figure 6. Software flowgraph.

The operation of the flowgraph is described by dividing it into separate logical blocks.

Preprints.org (www.preprints.org) | NOT PEER-REVIEWED | Posted: 21 April 2026 doi:10.20944/preprints202604.1500.v1

The first logical block, shown in Figure 7, is intended for the transmission and reception of radio signals.

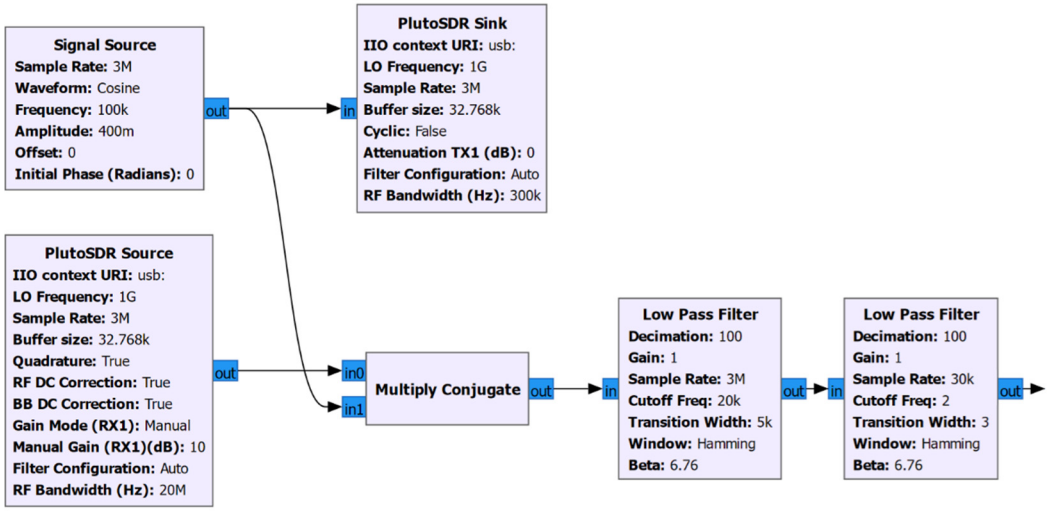

Figure 7. Block diagram of the transceiver section.

The Signal Source block generates with a sampling rate of $f_s = 3$ MHz an auxiliary complex sinusoidal signal of frequency $f_{BB} = 100$ kHz.

In the PlutoSDR Sink transmitter block, the signal at frequency f_{BB} is upconverted to the carrier frequency of the local oscillator $f_{LO} = 1$ GHz. As a result, a radio signal at 1.0001 GHz is formed and transmitted by the Adalm-Pluto device via a coaxial cable to the transmitting antenna.

The PlutoSDR Source receiver block receives the signal from the receiving antenna at the frequency 1.0001 GHz, downconverts it to the intermediate frequency of 100 kHz, and performs quadrature demodulation of the received radio-frequency signal.

In the Multiply Conjugate block, which functions as a mixer, the generated and received auxiliary signals at 100 kHz are multiplied.

To extract the low-frequency component corresponding to slow variations in amplitude and phase (breathing), a two-stage low-pass filtering is performed, with a cutoff frequency of 20 kHz in the first Low Pass Filter block and 2 Hz in the second Low Pass Filter block.

The second logical structure of the flowgraph, shown in Figure 8, is intended for displaying and recording information *about amplitude variations* of the signal during breathing.

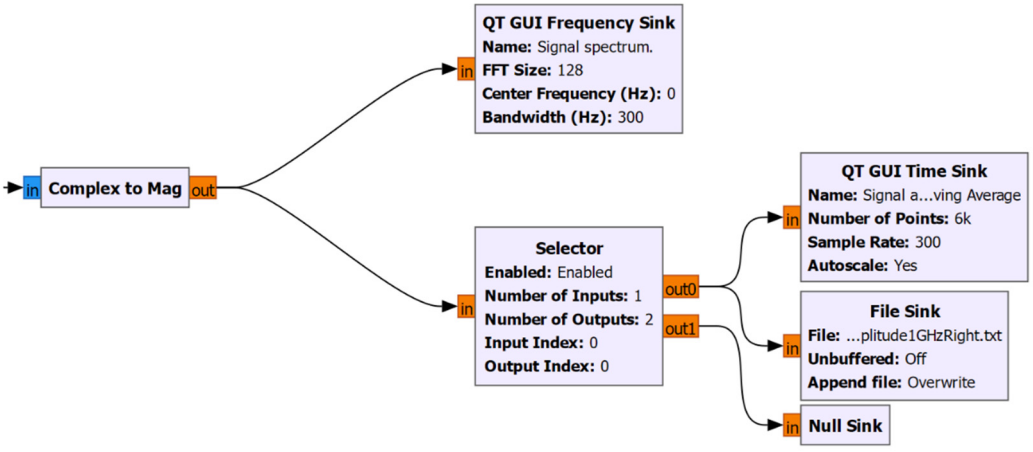

Figure 8. Block diagram for recording and displaying signal amplitude variations.

 doi:10.20944/preprints202604.1500.v1

The complex signal filtered by the low-pass filters, containing information about both amplitude and phase of signal, is fed into the Complex to Mag block, where only the amplitude information of the received signal is extracted. The time-varying signal is then fed to the QT GUI Frequency Sink block, which displays the spectrum of the received signal on the computer screen for operator monitoring, as well as to the Selector block. The Selector block waits for an event—specifically, the operator pressing the "START" button on the computer screen—and, upon this event, forwards the data to the QT GUI Time Sink block for visualization as a time-domain waveform, and to the File Sink block for recording the data to a file. The recording and visualization of data are stopped when the "STOP" button is pressed.

The third logical structure of the flowgraph, shown in Figure 9, is intended for displaying and recording information *about phase variations* of the signal during breathing.

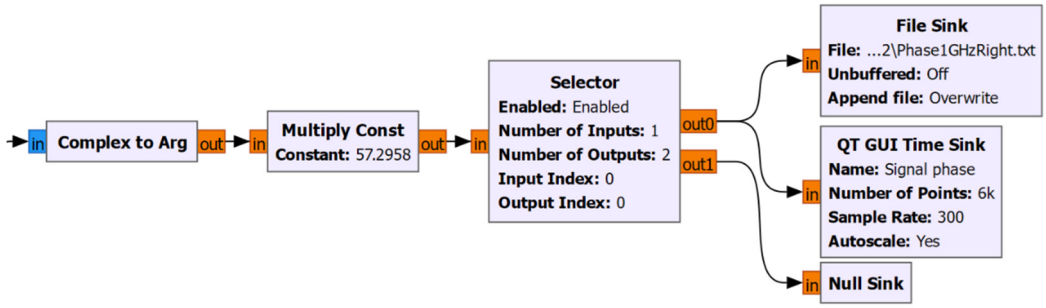

Figure 9. Block diagram for recording and displaying signal phase variations.

The complex signal filtered by the low-pass filters, containing information about both amplitude and phase of signal, is fed into the Complex to Arg block, where only the phase information of the received signal is extracted. The phase at the output of this block is represented in radians. To convert it into degrees, the signal is passed to the Multiply Const block, where all values are multiplied by the constant $\frac{180}{\pi} \approx 57.2958$. The time-varying phase signal is then fed to the QT GUI Frequency Sink block, which displays the spectrum of the received signal on the computer screen for operator monitoring, as well as to the Selector block. This block waits for an event—specifically, the operator pressing the "START" button—and, upon this event, forwards the data to the QT GUI Time Sink block for visualization as a time-domain waveform and to the File Sink block for recording the data to a file. Data recording and visualization of data are stopped when the "STOP" button is pressed.

To synchronize the operation of the measurement setup, a flowgraph shown in Figure 10 is provided.

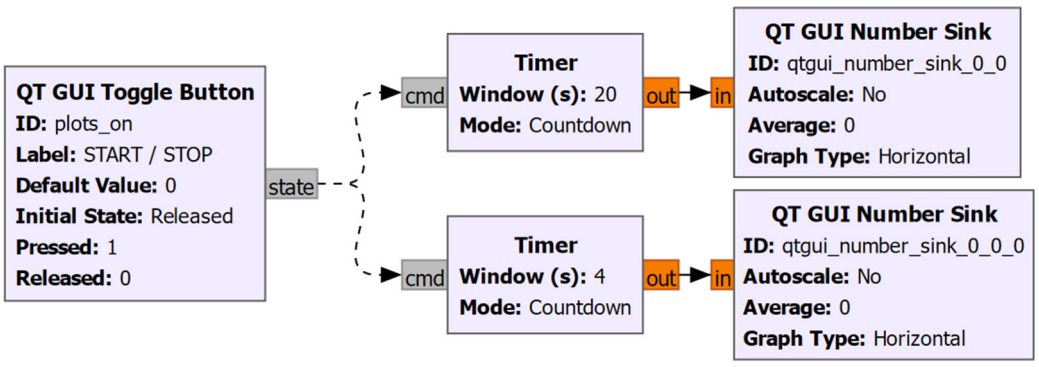

Figure 10. Synchronization block diagram.

This flowgraph includes two timers. The first timer (20 seconds) defines the update rate of the information on amplitude and phase variations of the signal during breathing. This allows several

 doi:10.20944/preprints202604.1500.v1

breathing cycles to be observed in the display window, which is useful for monitoring breathing dynamics. The second timer (set to 4 seconds in Figure 10) is adjusted by the researcher to match the average duration of inhalation/exhalation. This timer enables the subject (patient) to synchronize the breathing process. Its operation simulates the giving of "Inhale/Exhale" commands, making it possible to obtain relatively stable breathing intervals for implementing the technical solution described in the invention patent [17], aimed at improving the stability, informativeness and reliability of measurement results through joint processing of pulmonograms of different breathing cycles.

3. Results

The improved setup for radio-wave-based investigation of the breathing process proved to be compact and easy to operate. A large number of measurements were carried out using this setup to obtain *stable* and *repeatable* results.

In previous experiments, where a simplified physical model of the chest was used to interpret the results, a decrease in signal level during inhalation was expected. *Occasional* increases in signal level during inhalation *were considered* unreliable due to interference from reflected radio waves and movements of the human torso relative to the measurement antennas during the measurements.

After eliminating the causes of these errors, we nevertheless continued to obtain pulmonograms exhibiting different patterns of signal amplitude variations over the breathing cycle. For the experiments, pulmonograms were recorded over 20 breathing cycles in each measurement series. Synchronization signals ("inhale/exhale") were generated every 4 seconds. In practice, healthy subjects were able to follow this breathing rhythm without difficulty. However, for weakened patients, this rate was sometimes too slow. Therefore, the software was further modified to support shorter breathing cycles more suitable for patients. Nevertheless, in the present study, pulmonograms with an 8-second breathing period were used.

The considered model of electromagnetic wave propagation in the human body shows that *multiple* factors simultaneously influence the amplitude and phase variations of the signals, which can lead to diverse forms of pulmonograms. As an example, two pulmonograms obtained from the same subject are presented.

Figure 11 shows the amplitude and phase of the first four (out of twenty) breathing cycles of the pulmonogram measured at a frequency of $f = 10^9$ Hz, approximately at the mid-right region of the chest.

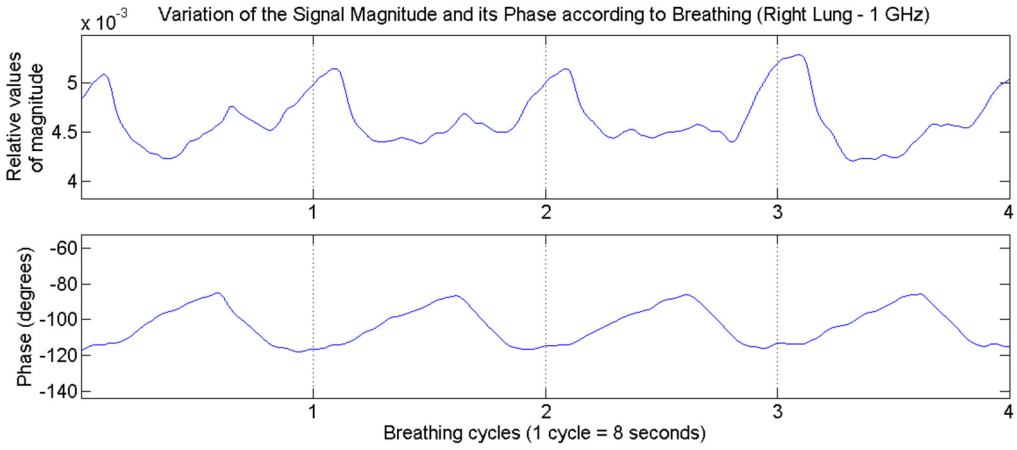

Figure 11. Pulmonogram of the *right lung*.

Figure 12 shows the amplitude and phase of the first four (out of twenty) breathing cycles of the pulmonogram measured at a frequency of $f = 10^9$ Hz, approximately at the mid-left region of the chest.

 doi:10.20944/preprints202604.1500.v1

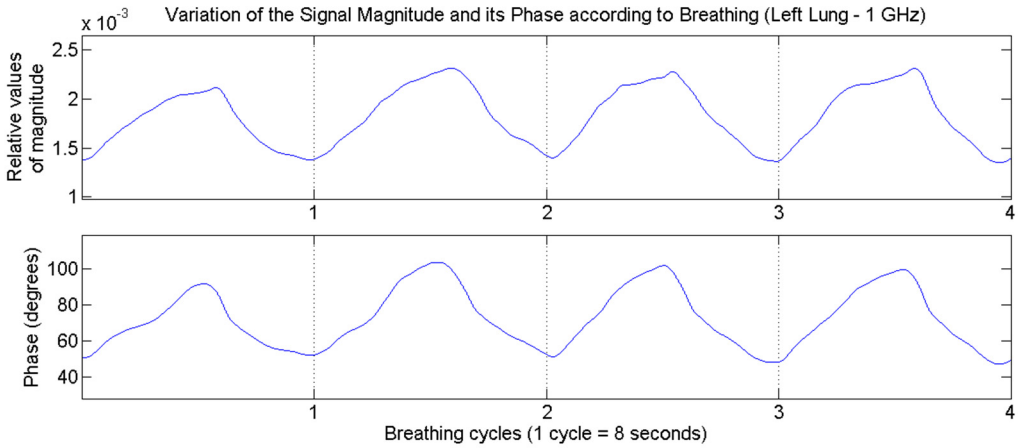

Figure 12. Pulmonogram of the *left lung*.

The amplitude information is presented in dimensionless relative units proportional to the received signal level (analog-to-digital converter (ADC) units). The phase information is presented in degrees. The variations of the radio signal amplitude and phase in Figures 11 and 12 are shown on the same scale.

For the calculations, data from all 20 recorded breathing cycles were used. The amplitude ratio was determined as the ratio between the maximum and minimum amplitude values over the 20 cycles. Similarly, the phase difference was calculated as the difference between the maximum and minimum recorded phase values.

The processing of the amplitude and phase components of the pulmonograms to separate them into contributions from the medium parameters and from chest motion was carried out using Equations (9) and (10), yielding the following results.

For the *right lung*, the logarithm of the ratio of the maximum to the minimum radio signal level is:

$$\ln \mathrm{Mag}_{ratio} = \ln \frac{5.7083 \times 10^{-3}}{2.2916 \times 10^{-3}} = 0.913$$

The difference between the maximum and minimum phase values is:

$$\mathrm{Ph}_{diff} = -77.032° - (-119.085°) = 42.05°$$

Attenuation coefficient during inhalation (11):

$$\alpha_{in} = \frac{23.45 \times 0.06 - 0.913}{0.07} = 7.06 \ {}^{\mathrm{Np}}/_{\mathrm{m}}$$

Wavenumber during inhalation (12):

$$\beta_{in} = \frac{151.50 \times 0.06 - \frac{\pi \times 42.05}{180}}{0.07} = 119.37 \ {}^{\mathrm{rad}}/_{\mathrm{m}}$$

Relative permittivity of the *right lung* during inhalation (15), calculated using the coefficients α_{in} and β_{in}:

$$\varepsilon_{r,\,in} = \frac{119.37^2 - 7.06^2}{(2\pi \times 10^9)^2 4\pi \times 10^{-7} \times 8.854 \times 10^{-12}} = 32.33$$

Decomposition of the value $\ln \mathrm{Mag}_{ratio}$ for the *right lung* into contributions from changes in the medium and changes in distance, according to Equation (9):

$$\ln \mathrm{Mag}_{ratio} = 0.913 \approx \ln(\mathrm{Mag}_{ratio})_{dist} + \ln(\mathrm{Mag}_{ratio})_{prop} =$$
$$= (-15.255 \times 0.01) + \big(-0.065(-16.39)\big) = (-0.15) + (1.07)$$

 doi:10.20944/preprints202604.1500.v1

Decomposition of Ph_{diff} into contributions from changes in the medium and changes in distance, according to Equation (10):

$$\mathrm{Ph}_{diff} = 42.05° \approx \mathrm{Ph}_{diff,\ dist} + \mathrm{Ph}_{diff,\ prop} =$$
$$= \left((-135.435 \times 0.01) + \left(-0.065 \times (-32.13)\right)\right)\frac{180}{\pi} = -77.60° + 119.66°$$

Attenuation coefficient during inhalation (11), associated with changes in the medium:

$$\alpha_{in,\ prop} = \frac{23.45 \times 0.06 - 1.07}{0.07} = 4.81\ {}^{\mathrm{Np}}/_{\mathrm{m}}$$

Wavenumber during inhalation (12), associated with changes in the medium:

$$\beta_{in,\ prop} = \frac{151.50 \times 0.06 - \frac{\pi \times 119.66}{180}}{0.07} = 100.02\ {}^{\mathrm{rad}}/_{\mathrm{m}}$$

Relative permittivity of the *right lung* during inhalation (15), after eliminating the contribution of chest motion, calculated using the coefficients $\alpha_{in,\ prop}$ and $\beta_{in,\ prop}$:

$$\varepsilon_{r,\ in} = \frac{100.02^2 - 4.81^2}{(2\pi \times 10^9)^2 4\pi \times 10^{-7} \times 8.854 \times 10^{-12}} = 22.72$$

For the *left lung*, the logarithm of the ratio of the maximum to the minimum radio signal level is:

$$\ln \mathrm{Mag}_{ratio} = \ln \frac{2.3706 \times 10^{-3}}{1.2578 \times 10^{-3}} = 0.6338$$

The difference between the maximum and minimum phase values is:

$$\mathrm{Ph}_{diff} = 103.658° - 43.000° = 60.66°$$

Attenuation coefficient during inhalation (11):

$$\alpha_{in} = \frac{23.45 \times 0.06 - 0.6338}{0.07} = 11.05\ {}^{\mathrm{Np}}/_{\mathrm{m}}$$

Wavenumber during inhalation (12):

$$\beta_{in} = \frac{151.50 \times 0.06 - \frac{\pi \times 60.66}{180}}{0.07} = 114.73\ {}^{\mathrm{rad}}/_{\mathrm{m}}$$

Relative permittivity of the *left lung* during inhalation (15), calculated using the coefficients α_{in} and β_{in}:

$$\varepsilon_{r,\ in} = \frac{114.73^2 - 11.05^2}{(2\pi \times 10^9)^2 4\pi \times 10^{-7} \times 8.854 \times 10^{-12}} = 29.69$$

Decomposition of the value $\ln \mathrm{Mag}_{ratio}$ for the *left lung* into contributions from changes in the medium and changes in distance, according to Equation (9):

$$\ln \mathrm{Mag}_{ratio} = 0.6338 \approx \ln(\mathrm{Mag}_{ratio})_{dist} + \ln(\mathrm{Mag}_{ratio})_{prop} =$$
$$= (-17.25 \times 0.01) + \left(-0.065(-12.40)\right) = (-0.17) + (0.81)$$

Decomposition of Ph_{diff} into contributions from changes in the medium and changes in distance, according to Equation (10):

$$\mathrm{Ph}_{diff} = 60.66° \approx \mathrm{Ph}_{diff,\ dist} + \mathrm{Ph}_{diff,\ prop} =$$
$$= \left((-133.115 \times 0.01) + \left(-0.065 \times (-36.77)\right)\right)\frac{180}{\pi} = -76.27° + 136.94°$$

Attenuation coefficient during inhalation (11), associated with changes in the medium:

$$\alpha_{in,\ prop} = \frac{23.45 \times 0.06 - 0.81}{0.07} = 8.53\ {}^{\mathrm{Np}}/_{\mathrm{m}}$$

Wavenumber during inhalation (12), associated with changes in the medium:

 doi:10.20944/preprints202604.1500.v1

$$\beta_{in,\ prop} = \frac{151.50 \times 0.06 - \frac{\pi \times 136.94}{180}}{0.07} = 95.71\ {}^{\mathrm{rad}}/_{\mathrm{m}}$$

Relative permittivity of the *left lung* during inhalation (15), after eliminating the contribution of chest motion, calculated using the coefficients $\alpha_{in,\ prop}$ and $\beta_{in,\ prop}$:

$$\varepsilon_{r,in} = \frac{95.71^2 - 8.53^2}{(2\pi \times 10^9)^2 4\pi \times 10^{-7} \times 8.854 \times 10^{-12}} = 20.69$$

Table 2 summarizes the main measurement results.

Table 2. Pulmonogram processing results.

Lung regions	Right lung	Left lung
Radio signal frequency during measurement	1 GHz	1 GHz
Logarithm of the ratio of the maximum to minimum radio signal level: $\ln \mathrm{Mag}_{ratio}$	0.91	0.63
Value of $\ln(\mathrm{Mag}_{ratio})_{prop}$	1.07	0.81
Difference between the maximum and minimum phase values: Ph_{diff}	42.05°	60.66°
Value of $\mathrm{Ph}_{diff,\ prop}$	119.66°	136.94°
Relative permittivity: $\varepsilon_{r,in}$	32.33	29.69
Relative permittivity after eliminating the contribution of chest motion: $\varepsilon_{r,in}$	22.72	20.69

The ability to measure not only amplitude but also phase pulmonograms has enabled a more accurate interpretation of the results. It has also made it possible to calculate the relative permittivity of the lungs during breathing, which may serve as a basis for the development of *diagnostic indicators*.

Another important outcome of this study is the evaluation of the accuracy of the measurement setup. The calculations presented above were performed using data from 20 breathing cycles, which represents a relatively long measurement duration at a single location. To assess the *minimum sufficient* number of cycles, the relative permittivity of the lungs $\varepsilon_{r,in}$ was calculated for different numbers of breathing cycles ranging from 1 to 20. For each number of cycles, 20 samples were obtained, and the corresponding values of relative permittivity were calculated.

Figure 13 shows the mean values and the variability (standard deviation) of the relative permittivity $\varepsilon_{r,in}$ of the right and left lungs during inhalation.

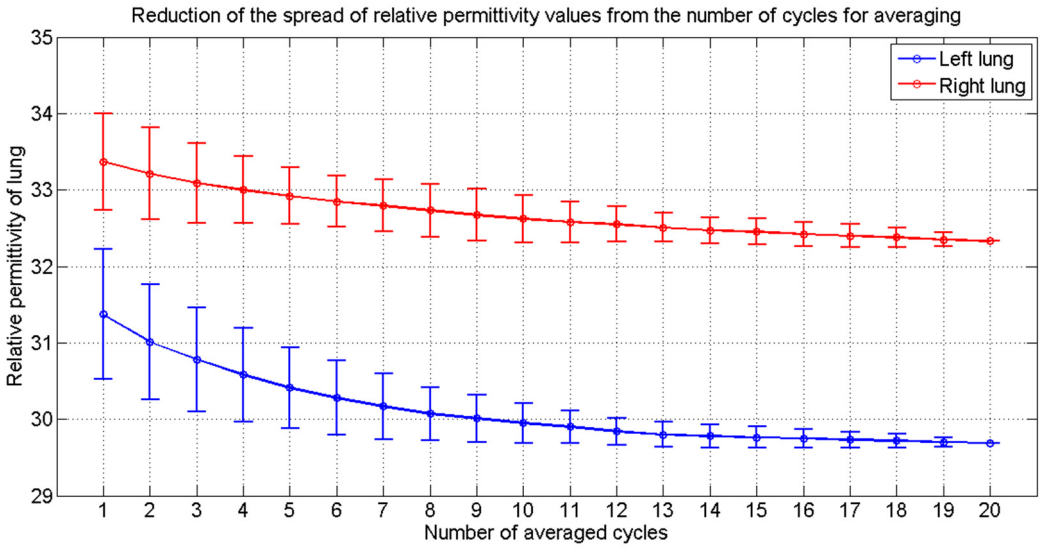

Figure 13. Mean values and variability (standard deviation) of the relative permittivity $\varepsilon_{r,in}$ for the right and left lungs.

 doi:10.20944/preprints202604.1500.v1

The results presented in Figure 13 indicate that even single breathing cycles can be used not only for qualitative but also for quantitative assessment of the relative permittivity of the lungs, which is directly *related* to the degree of lung air filling.

4. Discussion

Having demonstrated the feasibility of visualizing and imaging the lung air-filling process using a health-safe radio-wave method [13], we recognized that clinical medicine requires not merely a "qualitative" but a "quantitative" assessment of the degree of lung air filling. These numerical parameters can form the basis for diagnostic criteria. The relatively low signal-to-noise ratio observed in the initial experiments also hindered the clinical applicability of the proposed method [19].

Numerous experiments have confirmed the validity of the chosen approach to the development of the radio-wave diagnostic method, based on measuring not only the amplitude but also the phase of radio waves. Fixing the antennas on the patient's body and reducing the receiver bandwidth to 2 Hz made it possible to significantly improve the signal-to-noise ratio at the receiver output and to more clearly observe the dynamics of the measured parameters.

The addition of phase measurements to amplitude measurements enabled the calculation of the relative permittivity of the chest. This parameter, together with the geometrical dimensions of the chest, can serve as a basis for identifying clinical indicators of various bronchopulmonary diseases. This became possible due to the use of low-cost modern SDR transceiver devices. The cost of the equipment used in the experiments was several times lower than that used in the initial experiments (excluding the cost of the computer). This opens up prospects for applying the proposed method as a tool for rapid assessment of bronchopulmonary function during preventive examinations [31]. Moreover, it was found that the estimation of relative permittivity variation can be performed using a single breathing cycle.

A significant challenge remains the selection of measurement points. While in the acoustic domain pulmonologists perform measurements at auscultation points located near the bronchi, these locations are less informative for the radio-wave method. The method does not detect wheezes, but rather the degree of air filling of the alveoli. In future work, it is planned to provide a rigorous justification for optimal measurement locations for assessing air filling in different lobes of the lungs.

Another direction for future research aimed at improving the informativeness of pulmonograms is the use of simultaneous multi-frequency measurements. As follows from Equations (3) and (4), the coefficients α and β depend on the radio signal frequency. At the same time, the geometrical dimensions of the lungs cannot depend on this frequency. This implies that, when the geometrical dimensions are treated as approximate (as was done in this study), measurements at different frequencies will yield different values of relative permittivity. In reality, however, the relative permittivity of biological tissues varies only slightly within these frequency ranges. Therefore, the pulmonogram processing algorithm can be designed in such a way that, using successive iterative approximations and varying the parameters of lung dimensions and their variations, the corresponding values of these quantities can be estimated.

The analytical formulas used in this study were derived under the assumption that no resonant electromagnetic scatterers are present in the chest. Tumor formations may act as such scatterers [32–34]. The presence of frequency-dependent anomalies in the calculated relative permittivity at different frequencies may serve as an indicator of tumor formations and provide information about their size, since maximum scattering occurs when the wavelength of the radio signal is comparable to the size of the inhomogeneity.

It is possible that the parameter "relative permittivity" may not be the most convenient for clinicians. Terms related to the degree of lung air filling may be more intuitive for medical practitioners. The introduction of the term "air filling" was considered, but we regard this terminology as debatable. It may be preferable to adopt one of the terms commonly used in spirometric studies. Alternatively, the geometric dimensions of the lungs at the measurement locations during different stages of the breathing cycle may prove to be more practical.

 doi:10.20944/preprints202604.1500.v1

The large number of measurement samples performed by the system within a single breathing cycle enables the estimation of relative permittivity and geometric dimensions of the lungs not only over the entire cycle but also for each individual measurement samples. This allows for a more detailed analysis of the lung aeration process.

The compact size and low weight of the setup may facilitate the development of a device for screening examinations of the bronchopulmonary system.

5. Conclusions

The ability to measure the signal phase in addition to its amplitude enables the estimation of the relative permittivity of the lungs during breathing. Although the geometric dimension of the lung along the path between the transmitting and receiving antennas cannot be measured directly, this parameter can be estimated iteratively when measurements are performed at multiple frequencies. This direction of further research is promising for the development of diagnostic indicators of diseases.

Fixing the antennas on the patient's body and reducing the receiver bandwidth significantly improved the signal-to-noise ratio in radio-wave measurements. This makes it possible to perform measurements within a single breathing cycle, which is acceptable for real clinical practice, without the need for averaging over multiple cycles.

The issue of selecting optimal antenna placement points for obtaining diagnostically relevant information remains unresolved. Significant progress in this area is unlikely in the near future. It is necessary to involve additional research groups to collect statistically significant data across various types of diseases. The antenna fixation method used in this study enables the exploration of optimal antenna placement points. This approach is easy to implement and can be readily adopted by other researchers.

The use of low-cost and compact USRP device, together with the freely available GNU Radio framework, makes radio-wave monitoring systems accessible to researchers. Based on this platform, it is possible to develop a device for screening assessments of lung function not only in clinical settings but also during patients' normal daily activities.

Author Contributions: Conceptualization, Zhassulan Mendakulov; Data curation, Gulstan Yessetova and Kaiyrtay Issabayev; Formal analysis, Ivan Vassilyev and Gulstan Yessetova; Funding acquisition, Zhassulan Mendakulov; Investigation, Zhassulan Mendakulov and Ivan Vassilyev; Methodology, Zhassulan Mendakulov, Ivan Vassilyev and Gulstan Yessetova; Project administration, Zhassulan Mendakulov; Resources, Gulstan Yessetova and Kaiyrtay Issabayev; Software, Zhassulan Mendakulov; Supervision, Zhassulan Mendakulov; Validation, Ivan Vassilyev, Gulstan Yessetova and Kaiyrtay Issabayev; Visualization, Zhassulan Mendakulov and Kaiyrtay Issabayev; Writing – original draft, Zhassulan Mendakulov; Writing – review & editing, Ivan Vassilyev.

Funding: This research is funded by the Science Committee of the Ministry of Science and Higher Education of the Republic of Kazakhstan (Grant No. AP23488582)

Institutional Review Board Statement: Not applicable

Informed Consent Statement: Informed consent was obtained from all subjects involved in the study.

Data Availability Statement: The necessary data are available from the corresponding author upon reasonable request.

Conflicts of Interest: The authors declare no conflicts of interest.

 doi:10.20944/preprints202604.1500.v1

References

1. Xie, M.; Liu, X.; Cao, X.; Guo, M.; Li, X. Trends in prevalence and incidence of chronic respiratory diseases from 1990 to 2017. *Respiratory Research* **2020**, *21*, 49. https://doi.org/10.1186/s12931-020-1291-8
2. Luke, T. Covid-19: True global death toll from pandemic is almost 15 million, says WHO. *BMJ: British Medical Journal* **2022**, *377*, o1144. https://doi.org/10.1136/bmj.o1144
3. Martini, M.; Gazzaniga, V.; Bragazzi, N.L.; Barberis, I. The Spanish Influenza Pandemic: a lesson from the history 100 years after 1918. *Journal of Preventive Medicine and Hygiene* **2019**, *60*(1), E64-E67. https://doi.org/10.15167/2421-4248/jpmh2019.60.1.1205
4. Matteelli, A.; Saleri, N. Respiratory Diseases. In: *Travel Medicine* (Second Edition), Mosby **2008**, Chapter *57*, 561-572. https://doi.org/10.1016/B978-0-323-03453-1.10057-4
5. Zahar, J.-R.; Azoulay, E.; Klement, E.; De Lassence, A.; Lucet, J.-C.; Regnier, B.; Schlemmer, B.; Bedos, J.-P. Delayed treatment contributes to mortality in ICU patients with severe active pulmonary tuberculosis and acute respiratory failure. *Intensive Care Medicine* **2001**, *27*, 513–520. https://doi.org/10.1007/s001340000849
6. Lu, H.-H.; Zeng, H.-H.; Chen, Y. Early chronic obstructive pulmonary disease: A new perspective. *Chronic Diseases and Translational Medicine* **2021**, *7*, 79-87. https://doi.org/10.1016/j.cdtm.2021.02.003
7. Miravitlles, M.; Andreu, I.; Romero, Y.; Sitjar, S.; Altés, A.; Anton, E. Difficulties in differential diagnosis of COPD and asthma in primary care. *British Journal of General Practice* **2012**, *62*(595), e68-75. https://doi.org/10.3399/bjgp12X625111
8. Porter, P.; Brisbane, J.; Tan, J.; Bear, N.; Choveaux, J.; Della, P.; Abeyratne, U. Diagnostic Errors Are Common in Acute Pediatric Respiratory Disease: A Prospective, Single-Blinded Multicenter Diagnostic Accuracy Study in Australian Emergency Departments. *Frontiers in Pediatrics* **2021**, *9*, 736018. https://doi.org/10.3389/fped.2021.736018
9. Georgakopoulou, V.E.; Spandidos, D.A.; Corlateanu, A. Diagnostic tools in respiratory medicine (Review). *Biomedical Reports* **2025**, *23*(1), 112. https://doi.org/10.3892/br.2025.1990
10. Sang, L.; Zhao, Z.; Lin, Z.; Liu, X.; Zhong, N.; Li, Y. A narrative review of electrical impedance tomography in lung diseases with flow limitation and hyperinflation: methodologies and applications. *Annals of Translational Medicine* **2020**, *8*(24), 1688. http://dx.doi.org/10.21037/atm
11. Pedersen, P.C.; Johnson, C.C.; Durney, C.H.; Bragg, D.G. Microwave Reflection and Transmission Measurements for Pulmonary Diagnosis and Monitoring. *IEEE Transactions on Biomedical Engineering* **1978**, BME-25(1), 40-48. https://doi.org/10.1109/TBME.1978.326376
12. Semernik, I.V.; Demyanenko, A.V.; Semernik, O.E.; Lebedenko, A.A. Non-invasive method for bronchopulmonary diseases diagnosis in patients of all ages based on the microwave technologies. *2017 IEEE Conference of Russian Young Researchers in Electrical and Electronic Engineering (EIConRus)*, St. Petersburg and Moscow, Russia **2017**, 78-81. https://doi.org/10.1109/EIConRus.2017.7910497
13. Vassilyev, I.; Mendakulov, Z. Electromagnetic Imaging for Breathing Monitoring. *Sensors* **2024**, *24*(23), 7722. https://doi.org/10.3390/s24237722
14. Sadiku, M.N.O. Elements of Electromagnetics, 7th ed.; Oxford University Press: New York, NY, USA **2018**; pp. 480–481.
15. Sadiku, M.N.O. Elements of Electromagnetics, 7th ed.; Oxford University Press: New York, NY, USA **2018**; p. 481.
16. Zhang, H.; Li, M.; Yang, F.; Xu, S. A feasibility study of microwave respiration monitoring. *2017 Sixth Asia-Pacific Conference on Antennas and Propagation (APCAP)*, Xi'an, China **2017**, 1-3. https://doi.org/10.1109/APCAP.2017.8420537
17. Patent for invention. Vassilyev, I.V.; Mendakulov, Z.K.; Adamov, T.N.; Berdimuratova, L.B.; Nikitin, V.V.; Abdullayev, T.K.; Troitskaya, N.I. Microwave system for monitoring of bronchopulmonary system functioning. KZ Patent No. 36832, Jul. 5, **2024**. IPC A61B 5/0205, A61B 5/08, G01N 22/00. Assignee SDTB "Granit" (KZ). No. 2023/0374.1. Filed on May 31, 2023. Appl. No. 27. // URL: https://gosreestr.kazpatent.kz/Invention/Details?docNumber=376313

 doi:10.20944/preprints202604.1500.v1

18. ICNIRP – International Commission on Non-Ionizing Radiation Protection. RF EMFS 100 kHz – 300 GHz. Available online: URL: https://www.icnirp.org/cms/upload/publications/ICNIRPrfgdl2020.pdf Accessed 16 Apr. 2026
19. Vassilyev, I.V.; Mendakulov, Z.K. Increasing the informativeness of pulmonograms. *Biomedical Engineering* **2024**, *58*, 45–49. https://doi.org/10.1007/s10527-024-10363-6
20. Kaur, G.; Kaur, A.; Toor, G.K.; Dhaliwal, B.S.; Pattnaik, S.S. Antennas for biomedical applications. *Biomedical Engineering Letters* **2015**, *5*, 203-212. https://doi.org/10.1007/s13534-015-0193-z
21. Rafique, U.; Pisa, S.; Cicchetti, R.; Testa, O.; Cavagnaro, M. Ultra-Wideband Antennas for Biomedical Imaging Applications: A Survey. *Sensors* **2022**, *22*(9), 3230. https://doi.org/10.3390/s22093230
22. Li, X.; Jalilvand, M.; Sit, Y.L.; Zwick, T. A Compact Double-Layer On-Body Matched Bowtie Antenna for Medical Diagnosis. *IEEE Transactions on Antennas and Propagation*, *62*(4), 1808-1816. https://doi.org/10.1109/TAP.2013.2297158
23. Patent for utility model. Vassilyev, I.V.; Vyazigin, V.Y.; Mendakulov, Z.K.; Troitskaya, N.I. Antenna for biometric measurements. KZ Patent No. 10196, Feb. 14, **2025**. IPC H01Q 1/38. Assignee SDTB "Granit" (KZ). No. 2024/1659.2. Filed on Dec. 26, 2024. Appl. No. 7. // URL: https://gosreestr.kazpatent.kz/Utilitymodel/Details?docNumber=415092
24. Vassilyev, I.V.; Mendakulov, Zh.K.; Khachikyan, V.S.; Vasileva, O.I.; Yessetova, G.U. Choosing the optimal range of radio frequencies for measuring pulmonograms. *Meditsinskaya Tekhnika* **2025**, *5*, 43-45. http://mtjournal.ru/archive/2025/meditsinskaya-tekhnika-5/vybor-optimalnogo-diapazona-radiochastot-dlya-izmereniya-pulmonogramm (in Russian)
25. Șorecău, M.; Șorecău, E.; Bechet, P. Wideband Monitoring System of Drone Emissions Based on SDR Technology with RFNoC Architecture. *Drones* **2026**, *10*(2), 117. https://doi.org/10.3390/drones10020117
26. Toker, O.; Adla, R. A Sub-6 GHz Vital Signs Sensor Using Software Defined Radios. *Engineering Proceedings* **2020**, *2*(1), 38. https://doi.org/10.3390/ecsa-7-08197
27. Nguyen, T.-K.; Nguyen, N.D.; Nguyen, H.Q.; Nguyen, K.T.V. Signal Enhancement and Interference Reduction with Minimum-Variance Distortionless Response Algorithm Using MATLAB and GNU Radio Simulations. *Engineering Proceedings* **2025**, *92*(1), 73. https://doi.org/10.3390/engproc2025092073
28. Perotoni, M.B.; Huillery, J. Time Reversal Technique Experiments with a Software-Defined Radio. *Telecom* **2025**, *6*(4), 83. https://doi.org/10.3390/telecom6040083
29. Díez-García, R.; Camps, A. Adaptive near Real-Time RFI Mitigation Using Karhunen–Loève Transform. *Remote Sensing* **2025**, *17*(15), 2578. https://doi.org/10.3390/rs17152578
30. Rehman, A.U.; Galluccio, L.; Morabito, G. AI-Driven Adaptive Communications for Energy-Efficient Underwater Acoustic Sensor Networks. *Sensors* **2025**, *25*(12), 3729. https://doi.org/10.3390/s25123729
31. Yessetova, G.U.; Mendakulov, Zh.K.; Tolegen, A.Zh.; Rakhimzhanova, B.T. A study of the airiness of the lungs using ultra-high-frequency radio waves for the purpose of visualizing the state of the bronchopulmonary system. *Phthisiopulmonology* **2026**, *01*(51), 44-56. https://doi.org/10.26212/2227-1937.2026.87.18.004 (in Russian)
32. Hamza, M.N.; Koziel, S.; Pietrenko-Dabrowska, A. Design and experimental validation of a metamaterial-based sensor for microwave imaging in breast, lung, and brain cancer detection. *Scientific Reports* **2024**, *14*, 16177. https://doi.org/10.1038/s41598-024-67103-9
33. Camacho, L.M.; Tjuatja, S. FDTD simulation of microwave scattering from a lung tumor. *2005 IEEE Antennas and Propagation Society International Symposium*, Washington, DC, USA **2005**, *3A*, 815-818. https://doi.org/10.1109/APS.2005.1552382
34. Khalesi, B.; Khalid, B.; Ghavami, N.; Raspa, G.; Ghavami, M.; Dudley-McEvoy, S.; Tiberi, G. A Microwave Imaging Procedure for Lung Lesion Detection: Preliminary Results on Multilayer Phantoms. *Electronics* **2022**, *11*(13), 2105. https://doi.org/10.3390/electronics11132105